Hindawi Publishing Corporation
Journal of Structures
Volume 2014, Article ID 216549, 17 pages
http://dx.doi.org/10.1155/2014/216549

*Research Article*

# Analytical Modeling of Masonry Infilled RC Frames and Verification with Experimental Data

**S. Skafida, L. Koutas, and S. N. Bousias**

*Department of Civil Engineering, University of Patras, Rio, 26500 Patras, Greece*

Correspondence should be addressed to S. Skafida; stavroula.sk@gmail.com

Received 30 September 2013; Accepted 5 February 2014; Published 22 April 2014

Academic Editor: Zhongwei Guan



The assessment of the response of masonry infilled RC frame structures has been a major challenge over the last decades. While several modeling approaches have been proposed, none can cover all aspects observed in the tests. The present paper introduces a simplified model built on the approach established by Crisafulli and Carr (2007) and addresses its calibration and implementation in a nonlinear analysis software for the evaluation of the in-plane lateral response of infilled RC frames. The proposed model uses a set of elements/springs to account separately for the compressive and shear behavior of masonry. The efficiency of the modeling approach is validated with available experimental data, yielding satisfactory matching. The most intricate issue encountered when attempting to represent a masonry panel is the plethora of the material parameters involved and the lack of complete and available test results. Thus, the numerical investigation is accompanied by a parametric study on the sensitivity of the model to the various parameters to identify the critical modeling quantities and provide guidance on their selection.

## 1. Introduction

The evaluation of the seismic performance of masonry infilled RC frame structures is a widespread problem that has not yet been resolved despite the numerous efforts reported in the literature during the last decades. As a result, and contrary to the finding from the response of masonry infilled structures under actual seismic action, infill is often treated as nonstructural elements and is omitted by the analysis models. Nevertheless, the uncertainty associated with the interaction of the infill with the bounding frame and the different failure modes exhibited, the variability of the material properties, geometrical configurations, and construction methods reveal the complexity of the problem and justify the lack of unified, reliable, and widely accepted approaches for the design and assessment of structural systems that include infill panels.

From the computational point of view, the modeling techniques used for the analysis of infilled frames can be divided into two main categories: (i) local or micromodels and (ii) simplified macromodels. The first category is based on the nonlinear finite element method and strives to provide an accurate representation of the frame-infill interaction at the local level. Many of the researchers, who adopted this methodology, for example, Lotfi [2], Lourenco [3], Attard et al. [4], and Mehrabi and Shing [5], used a combination of continuum and interface line elements to simulate the fracture behavior of brick units and mortar joints. In Chiou et al. [6], infilled RC frames have been modeled by discretizing the brick units and concrete members into blocks interconnected with contact springs to account for the tensile and shear failure. One of the most recent studies on this field, conducted by Stavridis and Shing [7], combines the advantages of the smeared and discrete crack approaches to capture the different failure modes expected to occur either in the RC bounding frame elements or in the masonry panel. Although appealing, the complexity of the constitutive models incorporated in finite element analysis, involving intensive computational effort, hinders their application in the analysis of large structures.

On the other hand, macromodels utilize the "equivalent truss" concept to provide a simple and efficient tool, able to represent the global response of the infill panel and its interaction with the surrounding RC frame. The basic idea of this family of models was first suggested by Polyakov [8] and lies in the observation that when subjected to lateral loads the infill wall tends to separate from the bounding

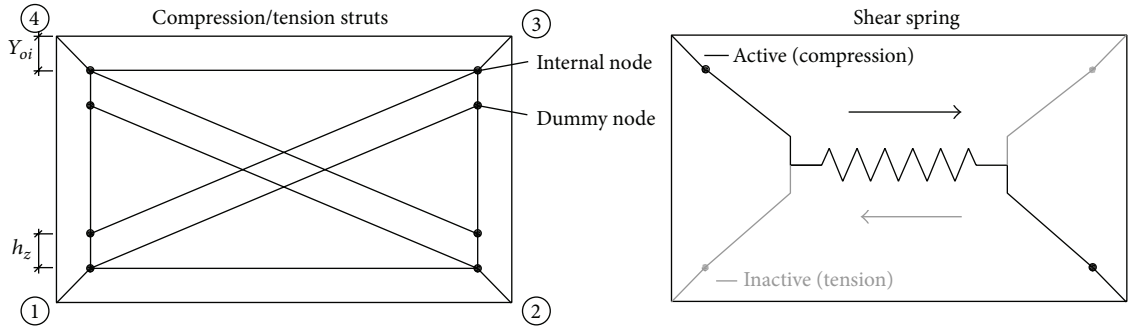


Figure 1: Schematic representation of the Crisafulli and Carr masonry panel element [1].

frame at a relatively low drift level, forming a resistance mechanism similar to that of a diagonal strut connecting the two opposite compression corners where contact with the frame is still retained. Various studies have been conducted in order to define the appropriate modeling configuration, the properties, and the constitutive law of the equivalent struts. Some of the earlier works in this area, like the investigations conducted by Holmes [9], Smith [10], and Mainstone [11], considered a single strut connecting the corner nodes along each diagonal and tried to evaluate the width of the strut that controls the initial stiffness of the infilled frame. Others who worked in the same direction refined the modeling technique, either by introducing multiple strut configurations to allow a more reliable estimation of the interaction between the panel and the frame (e.g., [1, 12–14]) or by developing appropriate constitutive laws to describe the hysteretic behavior of the panel when subjected to cyclic loading. The hysteretic rules developed by Fardis and Panagiotakos [15] to model the global behavior of the infill and the constitutive model proposed by Crisafulli [16] to describe the cyclic response of axially loaded masonry are two of the more interesting approaches in this regard.

Summarizing the available solutions, it seems that even if macromodeling schemes are not capable of simulating in a detailed manner all the possible failure mechanisms encountered in infilled frame structures, the limited computational effort required for their implementation makes them the best alternative, especially when analyzing large structures. The challenge is, yet, to develop a broadly applicable framework for determining the effective properties and the hysteretic behavior of the appropriate simplified model for each case study.

The aim of this paper is to provide an analytical tool for assessing the in-plane behavior of masonry infilled RC frames, focusing on the establishment of a set of specific guidelines for the evaluation of the various parameters required to define the monotonic and hysteretic response of the masonry infill. The modeling scheme presented herein constitutes a modification of the "masonry-panel" approach, originally developed by Crisafulli and Carr [1]. The proposed methodology has been validated with experimental results from masonry infilled RC frames subjected to in-plane cyclic quasi-static loading histories. Five of the experimental studies considered are presented in this paper to demonstrate the implementation procedure and the efficiency of the model. Additionally, an extensive parametric study has been conducted to clarify the influence of the various parameters on the overall structural response.

## 2. Materials and Methods

*2.1. Proposed Modeling Scheme.* As previously mentioned, the modeling scheme presented in this study is based on the "masonry-panel" model proposed by Crisafulli and Carr [1] that is a 4-node panel element connected to the frame at the beam-column joints. Internally, the panel element consists of two parallel struts and a shear spring acting in each diagonal (Figure 1), to account for both the compressive and the shear behavior of the masonry panel. Encapsulation of the multiple springs involved in the definition of the model into a 4-node element serves to establish an interrelation between the compressed diagonal and the shear spring, while reducing the level of complexity from the user's point of view. Still, this convenience also results in a limited control and some sort of obscurity behind the several parts that comprise the panel and define its behavior.

The configuration of the model as presented here maintains the idea of combining diagonal strut and shear spring elements with the difference that no interrelation between the individual elements that comprise the panel has been externally imposed, except the one arising from the distribution of strength and stiffness among the various components during a loading event. As the original model by Crisafulli was not available in the software framework used in this study (*OpenSees*), the scope of this research was limited to relaxing a number of parameters in the original model and checking if the resulting approach can reliably predict the experimental results. Thus, the infill is modeled here employing two "struts," each one connecting the two opposite diagonal corners of the panel, and a "shear spring" as shown in Figure 2. The behavior of each element is controlled by its own constitutive law—here a different constitutive law is assigned to the shear spring, with respect to that of the model by Crisafulli.

The model has been implemented in *OpenSees* [17], using the existing "two-node link" element (Figure 3). The element connects two diagonally opposite nodes and can generally comprise from 1 to 6 degrees of freedom, where only the

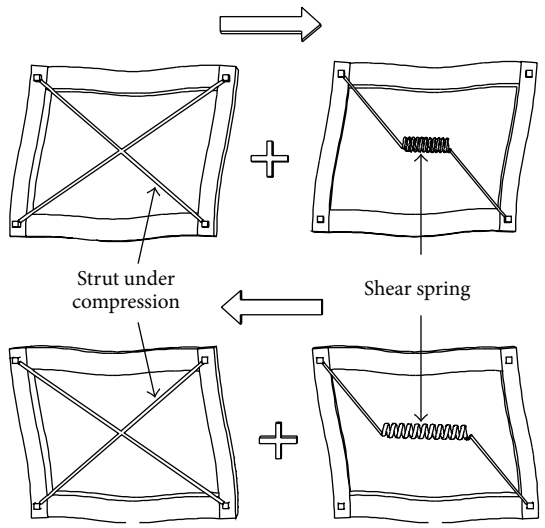


Figure 2: Schematic representation of the proposed model (modification of [1]).

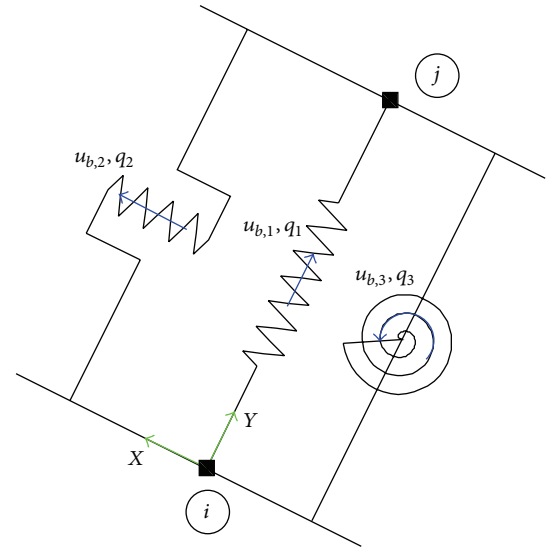


Figure 3: Generic representation of the "two-node link element," *OpenSees* framework.

transverse and rotational DOFs are coupled, as long as the element has a nonzero length. The behavior in each direction is defined by a specific material model.

In this particular modeling scheme, the struts are modeled with "two-node link" objects connecting the opposite corner nodes of the panel that are active solely in the direction of the diagonal. As far as the shear spring is concerned, it is modeled with a "two-node link" object that connects two of the opposite corner nodes of the panel and acts in the horizontal direction. In the proposed formulation, the shear spring represents only part of the response of the infill panel in shear and does not contribute to the axial force assumed by the columns.

For the numerical simulation of the RC frame member, a nonlinear fiber-based element formulation was selected. A "force based beam column" element with several (usually 6 to 8) integration points along its height was used to model each beam/column member. The model takes into account the interaction between axial and bending forces, but it is incapable of representing the shear behavior of the frame members.

### 2.2. Constitutive Material Models

*2.2.1. Concrete and Reinforcing Steel Material Models.* The material models employed in the inelastic fiber-based elements for the numerical simulation of RC frame components are available in the *OpenSees* framework. More specifically, "*Concrete02*" and "*Steel02*" were employed to model the concrete and the reinforcing bar fibers, respectively. The properties of the confined concrete core in beam and column elements are determined by the constant-confinement model of Mander et al. [18]. Bond-slip conditions at overlapping regions are not taken into consideration in the present study.

*2.2.2. Cyclic Compression/Tension Strut Relation.* The axial force-deformation relationship developed by Crisafulli [16], to describe the behavior of masonry under axial cyclic loading, was regarded as the most suitable alternative for the diagonal struts. The hysteresis rules describing the model were coded in *OpenSees* to yield a new material model. An analytical description of the model can be found elsewhere [16]. Nevertheless, some of the hysteretic modeling aspects will be presented in brief, so that the reader becomes familiar with some basic concepts discussed later.

The constitutive law for the axial cyclic behavior of the strut is expressed in terms of stress-strain relationships (Figure 4). Six material parameters are required to define the envelope curve in compression, namely, (i) initial modulus of elasticity, $E_{\text{mo}}$; (ii) compressive strength, $f'_m$; (iii) tensile strength, $f'_t$; (iv) strain at maximum stress, $\varepsilon'_m$; (v) ultimate strain, $\varepsilon_{\text{ult}}$; and (vi) closing strain, $\varepsilon_{\text{cl}}$, which defines the strain at which the cracks partially close allowing compression stresses to develop. In addition to these mechanical material parameters, a set of nine empirical factors associated exclusively with the hysteretic response need to be defined. The empirical factors and a short explanation of their significance are given here.

$G_{\text{un}}$ defines the unloading modulus in proportion to the initial modulus, $E_{\text{mo}}$.

$A_{\text{re}}$ predicts the strain at which the loop reaches the envelope after unloading.

$A_{\text{ch}}$ predicts the strain at which the reloading curve exhibits an inflection point, controlling the "fatness" of the loops.

$B_a$ defines an auxiliary point used to determine the plastic deformation after complete unloading.

$B_{\text{ch}}$ predicts the stress at which the reloading curve exhibits an inflection point.

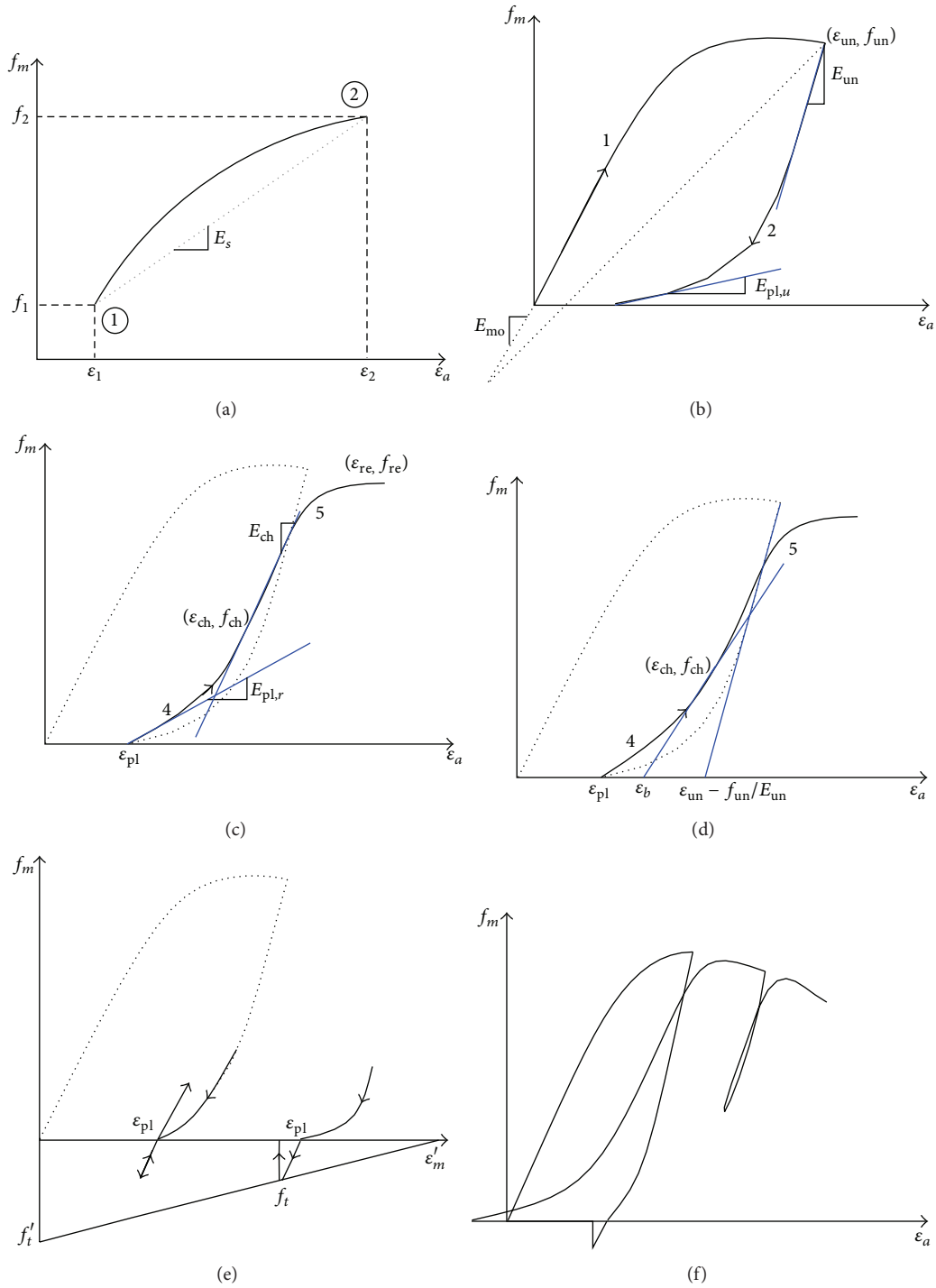


FIGURE 4: Cyclic response of axially loaded masonry proposed by Crisafulli [16]: (a) unloading and reloading rules, (b) Rule 1 for the envelope curve and Rule 2 for unloading, (c) Rules 4 and 5 for reloading, (d) definition of change point, (e) rule for tensile behavior, and (f) representation of the hysteretic model.

$G_{plu}$ defines the modulus of the hysteretic curve at zero stress after complete unloading in proportion to the initial modulus, $E_{mo}$.

$G_{plr}$ defines the modulus of the reloading curve after total unloading in proportion to the initial modulus, $E_{mo}$.

$e_1$ controls the influence of the strain at which unloading occurs, $\varepsilon_{un}$, in the degradation of stiffness.

$e_2$ increases the strain at which the envelope curve is reached after unloading and is used to control the cumulative damage inside repeated cycles.

Table 1: Suggested values proposed by Crisafulli [16] for the empirical parameters.

| Parameter | Suggested values | Limit values |
|---|---|---|
| $G_{un}$ | 1.5–2.5 | ≥0 |
| $A_{re}$ | 0.2–0.4 | ≥0 |
| $A_{ch}$ | 0.3–0.6 | 0.1–0.7 |
| $B_a$ | 1.5–2.0 | ≥0 |
| $B_{ch}$ | 0.6-0.7 | 0.5–0.9 |
| $G_{plu}$ | 0.5–0.7 | 0–1.0 |
| $G_{plr}$ | 1.1–1.5 | ≥1 |
| $e_1$ | 1.5–2.0 | ≥0 |
| $e_2$ | 1.0–1.5 | ≥0 |

Feasible ranges for all nine empirical parameters were suggested by Crisafulli [16] and are presented in Table 1.

The stress-strain relationship can be easily expressed in terms of the force-deformation quantities developed in the equivalent strut according to the following formulas:

$$F = \sigma A = \sigma(wt),$$
$$\delta_\alpha = \varepsilon L_{diag}, \quad (1)$$

where $w$ is the effective width of the diagonal strut, $t$ is the panel thickness, and $L_{diag}$ is the length of the strut.

An interesting characteristic of the model by Crisafulli is that the area of the equivalent strut is assumed to decrease with the increase in the lateral displacement (and consequently in the axial deformation of the strut), due to the reduction of the contact length between the panel and the frame and the development of extensive cracking in the panel. To account for this effect, the area (or equally the width) of the diagonal strut is assumed to vary as a function of the axial displacement, $\delta_\alpha$ (Figure 5).

*2.2.3. Cyclic Shear Spring Relationship.* The cyclic response of the shear spring used in the present model differs from the one adopted by Crisafulli et al. [1, 19] in that a simplification was introduced towards uncoupling the shear behavior from the axial compression in the struts, while the material model used to describe the behavior of the shear spring is the modified Ibarra-Medina-Krawinkler deterioration model ("*Bilin Material*" *in OpenSees*). Information on the model formulation can be found in Lignos and Krawinkler [20, 21].

The envelope of the modified IK model (Figure 6) is defined by six parameters: (i) the initial stiffness, $K_s$; (ii) yielding force, $F_y$; (iii) strain hardening ratio, $b$; (iv) precapping displacement capacity, $\delta_p$; (v) ultimate displacement, $\delta_{ult}$; and (vi) residual strength as a ratio, $\kappa$, of the yielding force.

The hysteretic response of the model follows a bilinear curve accounting for three modes of deterioration with respect to the backbone curve: (a) basic strength deterioration, (b) postcapping strength deterioration, and (c) unloading/reloading stiffness deterioration.

The rate of cyclic deterioration relates to the hysteretic energy dissipated during a cyclic event according to the proposal by Fardis [22]. The basic assumption is that every

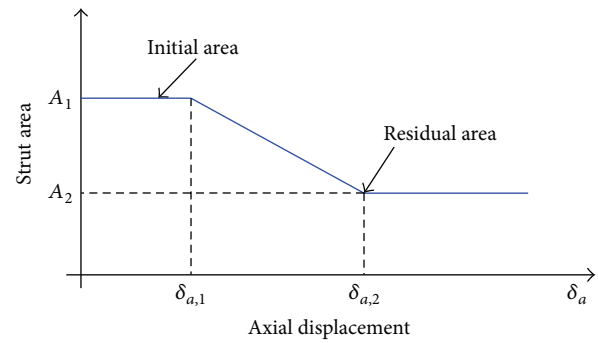


Figure 5: Variation of the area of the strut as a function of the axial displacement.

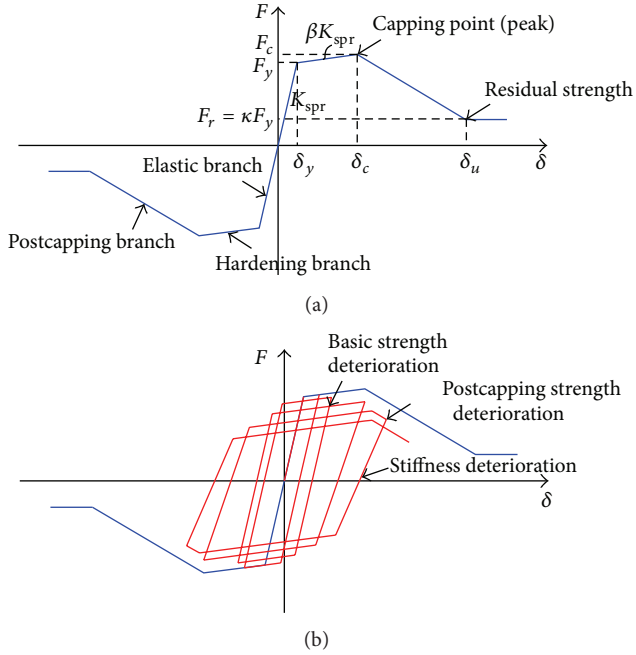


Figure 6: The Modified Ibarra-Krawinkler (IK) deterioration model: (a) monotonic curve and (b) basic modes of cyclic deterioration.

component has an inherent energy dissipation capacity, $E_t$, which can be expressed as a multiple of $(F_y \cdot \delta_p)$; that is,

$$E_t = (\lambda \delta_p) F_y = L \cdot F_y, \quad (2)$$

where $L$ is a reference cumulative displacement capacity and $\delta_p$ and $F_y$ are as defined previously.

Cyclic strength deterioration (either basic or postcapping) is modeled by translating the two strength bounds towards the origin at a rate equal to

$$F_i = \left[1 - \left(\frac{E_i}{E_t - \sum_{j=1}^{i-1} E_j}\right)^c\right] \cdot F_{i-1} = (1 - \beta_i) \cdot F_{i-1}, \quad (3)$$

where $\beta_i$ is an energy deterioration parameter, $E_i$ is the hysteretic energy dissipated in excursion $i$, $\sum E_j$ is the total

energy dissipated in past excursions, $E_t$ is the reference energy dissipation capacity, and $c$ is an empirical parameter.

The same concepts apply to modeling unloading stiffness deterioration.

In the present application of the model basic strength and stiffness deterioration are considered for capturing the shear behavior of the panel, by evaluating the appropriate values of $L$ and $c$ parameters for each deterioration mode. To account for the basic strength deterioration, $L_S$-values between 0.3 and 0.4 and $c$-values from 0.5 to 0.8 yield satisfactory results. The unloading stiffness deterioration parameter $L_K$ is inactive when assigned a very high value (for unloading with the elastic stiffness). Should the unloading stiffness deterioration be more pronounced, values in the range of 0.2–0.4 are suggested. Exponent $c_K$ is unit, for elastic unloading, or between 0.25 and 1.0, for soft unloading response. The influence of the deterioration parameters on the response of the panel will be clarified in the parametric study presented afterwards.

### 2.3. Evaluation of the Infill Material Properties

*2.3.1. Initial Stiffness.* For the evaluation of the initial stiffness of the masonry panel, the following formula suggested by Bertoldi et al. [23] has been adopted:

$$K_{\text{panel}} = \frac{G_m A}{H_{\text{panel}}} = \frac{G_m \left(L_{\text{panel}} t_{\text{panel}}\right)}{H_{\text{panel}}}, \tag{4}$$

where $L_{\text{panel}}$ is the clear length of the panel, $H_{\text{panel}}$ is the clear height of the panel, $t_{\text{panel}}$ is the panel thickness taken as equal to the thickness of the infill wall, and $G_m$ is the shear modulus of the masonry infill as determined from the wallette diagonal compression test (ASTM E519-81).

The total initial stiffness (defined in the horizontal direction) of the panel is shared between the shear spring and the diagonal struts according to the following expressions:

$$\begin{aligned} K_{\text{spr},h} &= \gamma \cdot K_{\text{panel}} = \gamma G_m \frac{L_{\text{panel}} t_{\text{panel}}}{H_{\text{panel}}}, \\ K_{\text{strut},h} &= (1-\gamma) \cdot K_{\text{panel}} = (1-\gamma) G_m \frac{L_{\text{panel}} t_{\text{panel}}}{H_{\text{panel}}}, \end{aligned} \tag{5}$$

where the parameter $\gamma$ defines the portion of the initial stiffness of the panel assigned to the shear spring. Its value usually ranges between 0.5 and 0.7.

Nevertheless, the initial stiffness of the diagonal strut element, expressed in the horizontal direction, is equal to

$$K_{\text{ini,strut},h} = \frac{E_{\text{mo}} w_1 t_{\text{panel}}}{L_{\text{strut}}} \cos^2\theta, \tag{6}$$

where $w_1$ is the initial effective width of the strut, $t_{\text{panel}}$ the masonry panel thickness, $L_{\text{strut}}$ the length of the diagonal strut, and $\theta$ the angle defined between the diagonal of the panel and the horizontal axis.

The initial modulus of elasticity assigned to the strut elements is derived through equating (5) and (6):

$$E_{\text{mo}} = (1-\gamma) G_m \left(\frac{L_{\text{strut}}}{w_1}\right)\left(\frac{L_{\text{panel}}}{H_{\text{panel}}}\right)\frac{1}{\cos^2\theta}. \tag{7}$$

Alternatively, the appropriate values for the parameters $\gamma$ and $E_{\text{mo}}$ can be evaluated through a repetitive procedure, so that the final value of $E_{\text{mo}}$ approximates the value calculated by the following expression, proposed by Pauley and Priestley [24]:

$$\begin{aligned} E_{\text{mo}} \approx E_{m\theta} = 1 \times \Bigg( &\frac{\cos^4\theta}{E_{\text{mh}}} + \frac{\sin^4\theta}{E_{\text{mv}}} \\ &+ \sin^2\theta\cos^2\theta\left(\frac{1}{G_m} - \frac{2\nu}{E_{\text{mh}}}\right)\Bigg)^{-1}, \end{aligned} \tag{8}$$

where $\nu$ is Poisson's ratio for the masonry panel and $E_{\text{mh}}$ and $E_{\text{mv}}$ are the elastic moduli for compression parallel and perpendicular to the bed joints, calculated via compressive tests on masonry prisms. As (8) requires the definition of three additional parameters, it is only presented here as an alternative way of obtaining $E_{\text{mo}}$.

*2.3.2. Shear Spring Yielding Strength and Hardening Ratio.* In the early stages of the response of a laterally loaded infilled frame, the infill panel acts as a shear wall, exhibiting substantially high lateral stiffness. However, as the infill panel deforms and the contact with the surrounding frame is limited to the vicinity of the beam-column joints, the lateral stiffness starts to degrade. In the present model, this high initial stiffness is attributed to the elastic branch of the shear spring response. Yielding of the shear spring is reached at a force level equal to a $a_1$-fraction of the infill cracking force, calculated according to the expression proposed by Panagiotakos and Fardis [15]. Hence the yielding force in the shear spring is

$$F_{\text{spr},y} = a_1 F_{\text{cr}} = a_1 \tau_{\text{cr}} L_{\text{panel}} t_{\text{panel}}. \tag{9}$$

Parameter $\alpha_1$ depends on the mechanical characteristics of the infilled frame; values between 0.25 and 0.35 yield reasonable results. Yielding is followed by a hardening branch of the backbone curve with a strain hardening ratio equal to $b = 0.05\%$.

*2.3.3. Strut Strength.* The compressive strength of the diagonal strut is estimated taking into account four possible failure mechanisms, as it was suggested by Pauley and Priestley [24]. The four basic failure modes encountered in infilled RC frames are (i) diagonal compression, (ii) crushing in the corners, (iii) sliding shear along the horizontal joints, and (iv)

diagonal tension. The corresponding resistances are obtained by

$$f_{m1} = \frac{1.16\tan\theta}{K_1 + K_2\lambda_h} f_{\mathrm{mv}},$$
$$f_{m2} = \frac{1.12\sin\theta\cos\theta}{K_1(\lambda_h)^{-0.12} + K_2(\lambda_h)^{0.88}} \tau_o,$$
$$f_{m3} = \frac{(1.2\sin\theta + 0.45\cos\theta)\,\tau_{\mathrm{cr}} + 0.3\sigma_v}{w/L_{\mathrm{diag}}}, \quad (10)$$
$$f_{m4} = \frac{0.6\tau_{\mathrm{cr}} + 0.3\sigma_v}{w/L_{\mathrm{diag}}},$$

where $f_{\mathrm{mv}}$ is the vertical compression strength measured on masonry specimens, $\tau_o$ is the shear bond strength measured from the triplet test, $\tau_{\mathrm{cr}}$ is the shear strength measured from the diagonal compression test, and $\sigma_v$ is the vertical stress acting on the masonry panel due to working loads. Parameters $K_1$ and $K_2$ depend on the relative panel-frame elements stiffness as expressed by parameter $\lambda$ and are taken according to Table 2.

The final compressive strength of the strut components is determined as the minimum of the four resistances calculated by (10); that is,

$$f'_m = \min\left(f_{m1}, f_{m2}, f_{m3}, f_{m4}\right). \quad (11)$$

The tensile strength of masonry is generally negligible compared to the value of compressive strength and is either assumed as nil or given a very small value (e.g., $f'_t = 0.05$ MPa adopted here).

*2.3.4. Initial and Reduced Area of the Strut.* A suitable value for the effective strut width has been sought by many researchers. Holmes [9] was the first to suggest that the equivalent strut width is equal to 1/3 of the diagonal length, while Pauley and Priestley [24] claimed that the value of 1/4 of the diagonal length is more appropriate. In the present study, the equations proposed by Decanini and Fantin [25] considering two different states of the infill wall are employed:

$$\frac{w_1}{L_{\mathrm{diag}}} = \left\{\begin{array}{l} 0.085 + \dfrac{0.748}{\lambda_h} \xrightarrow{\text{if}} \lambda_h \le 7.85 \\ 0.130 + \dfrac{0.393}{\lambda_h} \xrightarrow{\text{if}} \lambda_h > 7.85 \end{array}\right\} : \text{uncracked},$$
$$\frac{w_2}{L_{\mathrm{diag}}} = \left\{\begin{array}{l} 0.010 + \dfrac{0.707}{\lambda_h} \xrightarrow{\text{if}} \lambda_h \le 7.85 \\ 0.040 + \dfrac{0.470}{\lambda_h} \xrightarrow{\text{if}} \lambda_h > 7.85 \end{array}\right\} : \text{cracked}, \quad (12)$$

where $\lambda_h$ is the relative panel-to-frame stiffness parameter, calculated as

$$\lambda_h = H\sqrt[4]{\frac{E_m t_{\mathrm{panel}} \sin 2\theta}{4E_c I_c H_{\mathrm{panel}}}}, \quad (13)$$

Table 2: Parameters for the calculation of the compressive strength of the strut [23].

| | $\lambda h < 3.14$ | $3.14 < \lambda h < 7.85$ | $\lambda h > 7.85$ |
|---|---|---|---|
| $K_1$ | 1.3 | 0.707 | 0.47 |
| $K_2$ | −0.178 | 0.010 | 0.04 |

where $E_c$ and $I_c$ are the elastic modulus and the moment of inertia of the columns and $H$ is the height of the frame.

The area reduction factor used in the definition of the strut model is, therefore, determined as the ratio $A_{\mathrm{red}} = w_2/w_1$.

*2.3.5. Characteristic IDR-Levels of the Infill Response.* Interstorey drift level (IDR) is taken as the unifying parameter to connect the global deformation level to those of the diagonal struts and the shear spring, according to the following assumptions.

(i) There exists a characteristic interstorey drift level, $\mathrm{IDR}_1$, for which extensive cracks have been formed in the panel indicating the start of a higher rate of deterioration. Thus, it is assumed that $\mathrm{IDR}_1$ corresponds to the starting point of both the falling branch of the shear spring backbone curve and the reduction of the area of the compressive strut.

(ii) Interstorey drift level, $\mathrm{IDR}_2$, is related to the point where the area of the diagonal reaches its residual value, $A_2$.

(iii) Ultimate state conditions are considered at an interstorey drift level named $\mathrm{IDR}_3$, for which both the shear spring and the compressive diagonal strut have exhausted their resistance. It should be emphasized that the value of $\mathrm{IDR}_3$ is usually higher than the one observed during test events. This issue can be attributed to the fact that either some other kind of failure mechanism, related to the frame response (e.g., shear failures in the beam-column connections), has preceded the development of excessive damage on the infill or the experiment has been interrupted before the actual collapse of the panel.

The axial strain of the diagonal strut and the horizontal displacement of the shear spring can be related to the relevant drift level using the following expressions:

$$\delta = \mathrm{IDR} \cdot H,$$
$$\varepsilon = 1 - \sqrt{\frac{1 + ((L/H) - \mathrm{IDR})^2}{1 + (L/H)^2}}, \quad (14)$$

where $L$ and $H$ are, respectively, the length and height of the frame and $\mathrm{IDR} = \delta/H$, the interstorey drift ratio. The second expression, relating the axial strain in the strut to the IDR-level of the panel, is derived geometrically assuming that the vertical displacement at the beam-column joints is negligible. The shear spring and diagonal strut deformation quantities associated with the three IDR-levels defined above are summarized in Table 3.

Table 3: Dependence of shear spring and diagonal strut deformation quantities on the specified IDR-levels.

| IDR-level | Shear spring | Diagonal strut |
|---|---|---|
| $IDR_1$ | — | $\delta_{a,1}$ or $\varepsilon_{a,1}$ |
| $IDR_2$ | $\delta_c$ | $\delta_{a,2}$ or $\varepsilon_{a,2}$ |
| $IDR_3$ | $\delta_u$ | $\delta_{a,ult}$ or $\varepsilon_{a,ult}$ |

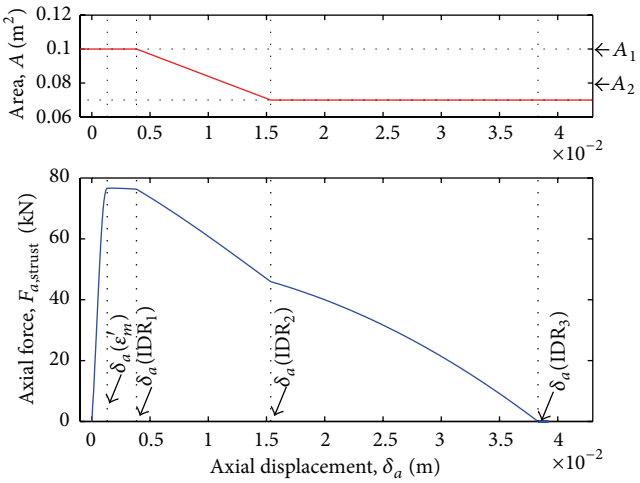


Figure 7: Compressive envelope in the diagonal strut, characteristic points of the force-deformation response, and variation of the effective area.

*2.3.6. Strain at Maximum Stress and Closing Strain on the Strut.* For completing the formulation of the model, two additional deformation quantities remain to be defined: (a) the axial strain at maximum stress and (b) the closing strain on the strut elements.

The axial strain, $\varepsilon'_m$, when the maximum stress is reached on the compressive strut, is an experimentally defined parameter. Since infilled frame systems display a steep initial branch to the peak strength, the value of the strain $\varepsilon'_m$ is relatively low, corresponding to a drift value within 0.01–0.05%.

As it was previously mentioned, the closing strain, $\varepsilon_{cl}$, represents the strain level in tension after which the cracks partially close allowing the development of compression stresses. According to Crisafulli [16], its value ranges from 0 to 0.003.

Figures 7 and 8 demonstrate the basic characteristics of their backbone curves described in the previous paragraphs, rendering the response of both the compressed strut and the shear spring during a monotonic pushover analysis of an infilled frame.

## 3. Model Application: Discussion of Results

*3.1. Experimental Data.* The predictions of the proposed approach are compared to a number of test results from masonry infilled RC frames subjected to quasi-static or cyclic displacement histories. Five of the investigated experiments are presented here to demonstrate the efficiency of the model. The first three are 2/3-scale models of one-storey single bay masonry infilled frames tested by Pires and Carvalho [26, 27]. The masonry units consisted of hollow clay bricks with dimensions 300 mm × 200 mm on the front side and 150 mm deep. In addition, the results from 2/3-scale model of a one-storey single bay infilled frame tested at the University of Colorado [28, 29] are used. In this case, a two-wythe masonry panel, made of solid clay bricks with dimensions 200 × 57 × 95 mm, was employed. Finally, the last experimental campaign regards a 2/3-scale model of a three-storey single bay infilled frame tested at the Structural Laboratory of the University of Patras [30]. The infill panel consisted of two single-wythe masonry walls with an internal gap of 60 mm. Perforated fired clay bricks with dimensions 185 × 85 × 55 mm were used for the construction of the infill. A cementitious mortar was used to fill the joints in all the above cases. The basic geometrical and mechanical properties of the specimens are reproduced in Tables 4 and 5.

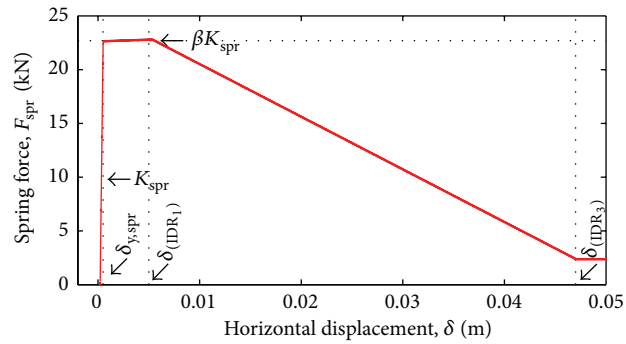


Figure 8: Shear spring envelope curve and characteristic points of the force-deformation response.

*3.2. Numerical Results.* The results obtained from the analysis of the above specimens are compared with the experimental results in terms of total base shear and interstorey drift, except for the test by Koutas et al. [30] for which the results are expressed in terms of base shear and total drift, calculated as the ratio of the top displacement to the total height of the structure, $IDR_{tot} = \delta_{top}/H_{tot}$. The parameters assigned to the strut and spring elements were evaluated according to the procedure described in Section 2.3 and all the assignments are summarized in Tables 6, 7, and 8.

The comparison of model predictions and experimental results is quantified via a dimensionless index, $f$, calculated as the fraction of the aforementioned difference in the force values to the maximum experimentally achieved base shear; that is,

$$\text{Index, } f = \frac{\left|F_i^{\text{anal.}}\right| - \left|F_i^{\text{exp.}}\right|}{\left|F^{\text{exp.}}\right|_{\max}} = \frac{\left|F_i^{\text{anal.}}\right| - \left|F_i^{\text{exp.}}\right|}{\left(\left(\left|F_{\max}^{\text{exp},(+)}\right| + \left|F_{\max}^{\text{exp},(-)}\right|\right)/2\right)}, \tag{15}$$

where the maximum value of the experimental base shear is calculated as the mean of the positive and negative shear

Table 4: Geometry of the investigated specimens.

| Specimen | $t_{panel}$ (mm) | $L$ (mm) | $H$ (mm) | $(b \times h)_{column}$ (mm) × (mm) | $(b \times h)_{beam}$ (mm) × (mm) | $A_{s,col}$ | $A_{s,beam}$ | $A_{sw}$ |
|---|---|---|---|---|---|---|---|---|
| Pires M2 | 150 | 2250 | 1825 | 150 × 150 | 150 × 200 | 8Φ8 | 3Φ8 (top)<br>3Φ8 (bot) | Φ4/50 |
| Pires M3 | 150 | 2250 | 1825 | 150 × 150 | 150 × 200 | 8Φ8 | 3Φ8 (top)<br>3Φ8 (bot) | Φ4/100 |
| Pires M6 | 150 | 2250 | 1825 | 150 × 150 | 150 × 200 | 4Φ8 | 3Φ8 (top)<br>3Φ8 (bot) | Φ4/50 |
| Colorado T1 | 190.5 | 3600 | 1930 | 280 × 280 | 240 × 280 | 8Φ11 | 2Φ19 (top)<br>2Φ19 (bot) | Φ6.4/267 |
| Koutas U1 | 110 | 2500 | 2000 | 170 × 230 | 170 × 330 | 6Φ12 | 2Φ12 (top)<br>2Φ12 (bot) | Φ6/130 |

Table 5: Material properties in the experimental studies considered.

| Specimen | $f_c$ (MPa) | $f_y$ (MPa) | $f_{yw}$ (MPa) | $G_m$ (MPa) | $\tau_{cr}$ (MPa) | $\tau_o$ (MPa) | $f_{vm}$ (MPa) |
|---|---|---|---|---|---|---|---|
| Pires M2 | 28.3 | 434 | 523 | 590 | 0.40 | 0.35 | 2.10 |
| Pires M3 | 33.2 | 434 | 523 | 590 | 0.40 | 0.35 | 2.10 |
| Pires M6 | 35.2 | 434 | 523 | 1000 | 0.51 | 0.40 | 2.30 |
| Colorado T1 | 30.1 | 458 | 458 | 2900 | 1.0* | — | 17.93 |
| Koutas U1 | 28.0 | 500 | 220 | 1620** | 0.90** | — | 5.07 |

Note: *the value of the parameter $\tau_{cr}$ was not available—the value was selected on the basis of satisfactory agreement with the analytical results.
Note: **$G_m$ and $\tau_{cr}$ have been evaluated on the basis of only 3 masonry prisms.

Table 6: Definition of IDR-levels for the selected specimens.

| Specimen | $IDR_1$ (%) | $IDR_2$ (%) | $IDR_3$ (%) |
|---|---|---|---|
| Pires M2 | 0.050 | 1.20 | 8.0 |
| Pires M3 | 0.021 | 0.60 | 8.0 |
| Pires M6 | 0.035 | 1.10 | 8.0 |
| Colorado T1 | 0.50 | 0.55 | 2.8 |
| Koutas U1 | 1.0 | 2.50 | 8.0 |

resistances. A close observation of the history of index $f$ allows a step-by-step investigation of the ability of the model to capture the actual response of the examined specimen. Four additional quantities are calculated to provide a more generic evaluation of the adequacy of the numerical simulation:

(i) the median of the positive $f$-values, offering an insight into the level of overestimation of the base shear;

(ii) the median of the negative $f$-values that reflects the level of underestimation of the base shear;

(iii) the maximum and the minimum $f$-values that provide a measure of the maximum error.

The previously defined quantities are computed on the remaining part of the data after excluding some low-level initial cycles (before the peak force is reached) and some of the final cycles for which shear effects on the frame elements were identified to dominate the response.

Another way to assess the efficiency of the proposed model is to compare the strain energy dissipated during each test with the dissipated energy calculated analytically. The cumulative dissipated strain energy, $S$, at step $i$ is computed according to the following formula:

$$S_i = S_{i-1} + \frac{1}{2}\left(R_i + R_{i-1}\right)\left(U_i - U_{i-1}\right), \tag{16}$$

where $S_{i-1}$ is the energy dissipated in previous steps, $R_i$ and $R_{i-1}$ are the base shear at two adjacent steps, and $U_i$ and $U_{i-1}$ are the corresponding top displacements. The average error between the cumulative strain energy dissipated in the model and the actual strain energy dissipated during the experiment is calculated as

$$\text{error} = \frac{\sum_{i=1}^{n} \left|S_i^{\text{anal}} - S_i^{\text{exp}}\right|}{\sum_{i=1}^{n} \left|S_i^{\text{exp}}\right|}. \tag{17}$$

The cumulative strain energy dissipated in the model is compared to the cumulative strain energy dissipated during the experiment in each of the examined specimens. Moreover, the error in the dissipated strain energy determined by (17) is used as a global measure of the accuracy of every numerical simulation.

In the following paragraphs, the comparative results obtained after interpreting the experimental and analytical data referring to each case study are presented and discussed. Generally, a smaller step-size was considered for the evaluation of the strain energy dissipation to allow a more

Table 7: Material properties assigned to the strut/spring elements for the selected specimens.

| Specimen | $f'_m$ (MPa) | $f'_t$ (MPa) | $(w/d)_{ini}$ | $(w/d)_{res}$ | $\varepsilon'_m$ | $\varepsilon_{cl}$ | $\gamma$ | $a_1$ |
|---|---|---|---|---|---|---|---|---|
| Pires M2 | −0.97 | 0.05 | 0.25 | 0.175 | −0.00013 | 0.002 | 0.6 | 0.3 |
| Pires M3 | −0.97 | 0.05 | 0.25 | 0.163 | −0.00010 | 0.002 | 0.6 | 0.3 |
| Pires M6 | −1.25 | 0.05 | 0.25 | 0.163 | −0.00013 | 0.002 | 0.6 | 0.3 |
| Colorado T1 | −2.55 | 0.05 | 0.27 | 0.189 | −0.00013 | 0.002 | 0.7 | 0.3 |
| Koutas U1 | −2.14* | 0.05 | 0.28 | 0.196 | −0.00050 | 0.002 | 0.7 | 0.3 |

*The compressive strength at 2nd/3rd floor is reduced to −2.07 MPa/−2.00 MPa, respectively, due to the lower level of axial stress (see Section 2.3.3).

Table 8: Empirical parameters assigned to the strut/spring elements for the selected specimens.

| Specimen | $A_{ch}$ | $A_{re}$ | $B_a$ | $B_{ch}$ | $G_{un}$ | $G_{plu}$ | $G_{plr}$ | $e_1$ | $e_2$ | $L_S$ | $L_K$ | $c_S$ | $c_K$ |
|---|---|---|---|---|---|---|---|---|---|---|---|---|---|
| Pires M2 | 0.3 | 1.5 | 1.0 | 0.9 | 0.7 | 1.0 | 1.1 | 3.0 | 1.0 | 0.3 | 1000 | 0.5 | 1.0 |
| Pires M3 | 0.3 | 1.5 | 1.0 | 0.9 | 0.5 | 1.0 | 1.1 | 3.0 | 1.0 | 0.3 | 1000 | 0.5 | 1.0 |
| Pires M6 | 0.3 | 1.5 | 1.0 | 0.9 | 0.7 | 1.0 | 1.1 | 3.0 | 1.0 | 0.3 | 0.20 | 0.9 | 1.0 |
| Colorado T1 | 0.3 | 0.8 | 1.0 | 0.9 | 0.5 | 1.0 | 1.1 | 3.0 | 1.0 | 0.4 | 0.20 | 0.6 | 0.25 |
| Koutas U1 | 0.3 | 0.8 | 1.0 | 0.9 | 0.7 | 1.0 | 1.1 | 3.0 | 1.0 | 0.3 | 0.25 | 0.5 | 1.0 |

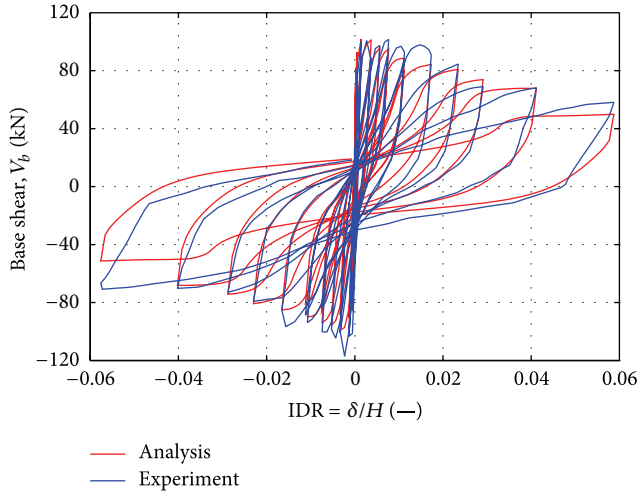


Figure 9: Pires M2 specimen.

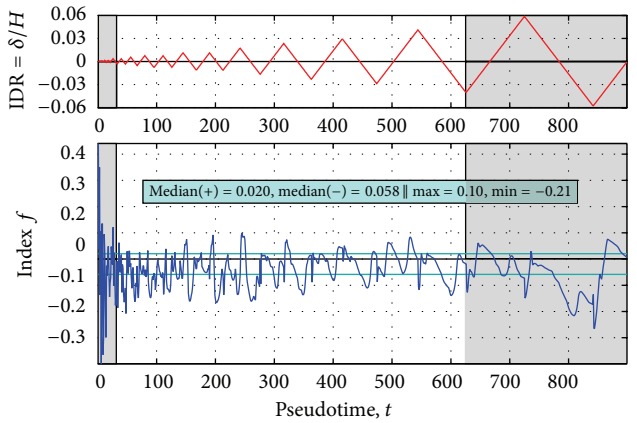


Figure 10: Variation of index $f$ for Pires M2 specimen.

accurate estimation of the area enclosed in the "Base shear-Displacement" loops, which explains the difference in the "pseudotime" measures in the relevant figures compared to the ones depicting the variation of index $f$.

Comparison of the analytically derived response for Pires M2 specimen with the corresponding experimentally obtained results (Figure 9) shows very good agreement. It is evident that both the shape of the hysteretic loops and the resistance of the infilled frame system are captured with acceptable accuracy. A more detailed interpretation of the results is achieved by observing the fluctuation of index $f$ throughout the displacement history (Figure 10). After omitting the shaded parts of the response (initial and final cycles), the level of overestimation of the base shear is calculated at 2% of the maximum experimental base shear value, while the level of underestimation is approximated at −5.8%, both indicating a very slight deviation from the experimental results.

The range of $f$-values (−0.21, 0.10) implies that the model exhibits greater differences from the experiment at some points of the response. These points are usually related to the initial phase of an unloading/reloading cycle, and they tend to diminish after a few steps. Differences are also noticed when the specimen is driven through the origin and until the diagonal strut that was previously loaded in tension develops substantial compressive stresses to contribute to the overall strength and stiffness.

As far as the cumulative strain energy dissipated by the infilled frame is concerned, it is generally underestimated in the numerical model (Figure 11). The average error calculated by (17) equals 14.9% which can be regarded as an acceptable difference.

Similar conclusions are drawn after evaluating the analytical results of specimen M3 by Pires. As depicted in Figure 12, the test showed an essentially asymmetric response, making the calibration of an analytical model and the investigation of its efficiency a difficult task. The level of underestimation in

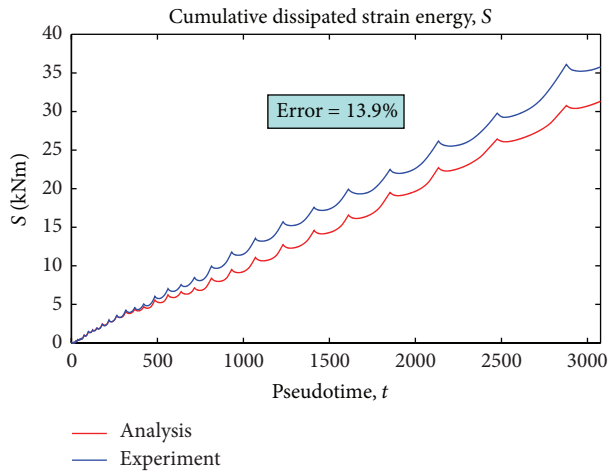


Figure 11: Cumulative strain energy comparison for Pires M2 specimen.

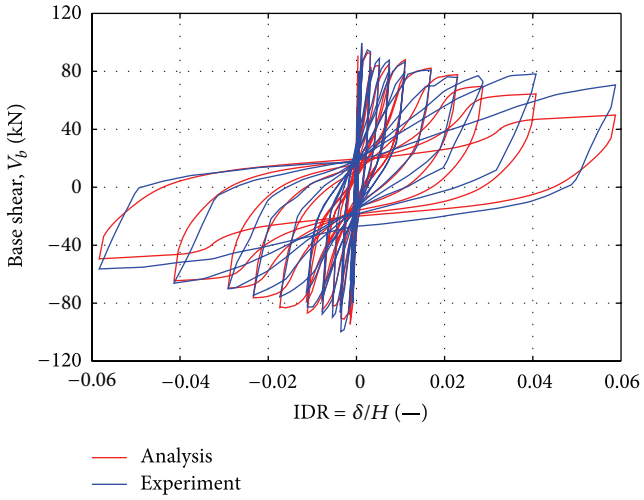


Figure 12: Pires M3 specimen.

this case is computed at −6.2% and the level of overestimation at 3.4% of the maximum experimentally obtained base shear. The range of index, $f$, is now evaluated at (−0.23, 0.17) as shown in Figure 13.

The cumulative strain energy, presented in Figure 14 for both the experiment and the analysis, is underestimated in the numerical model. The average error is 13.9%, slightly different from the corresponding error measured for specimen M2 by Pires.

Test M6 by Pires was also used, which, compared to the previous two specimens of the same research, features lighter reinforcement in the columns and stronger infill. The comparative results (Figures 15 and 16) provide evidence of satisfactory agreement between experimental data and model results. The values of the over- and underestimation indices result as 2.6% and −4.4%, respectively, while index $f$ falls within (−0.27, 0.10) range of values.

The cumulative strain energy dissipated in the numerical model is overestimated until a drift level of around

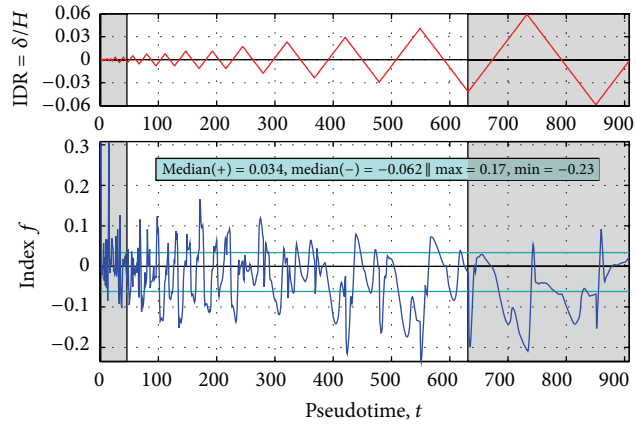


Figure 13: Variation of index $f$ for Pires M3 specimen.

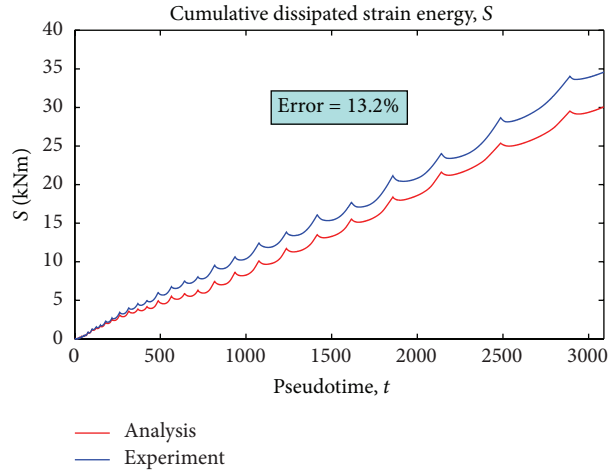


Figure 14: Cumulative strain energy comparison for Pires M3 specimen.

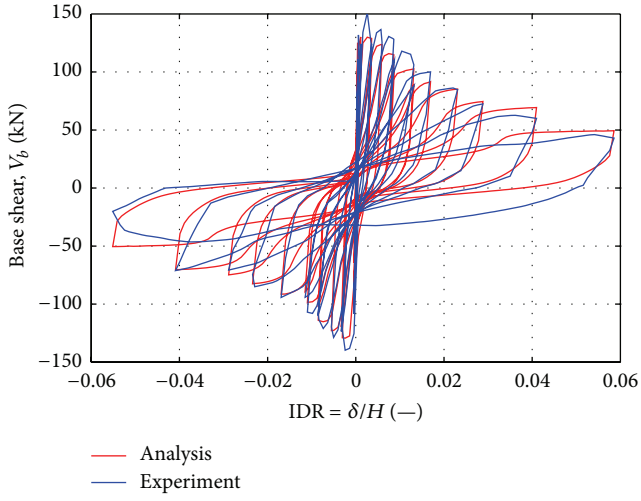


Figure 15: Pires M6 specimen.

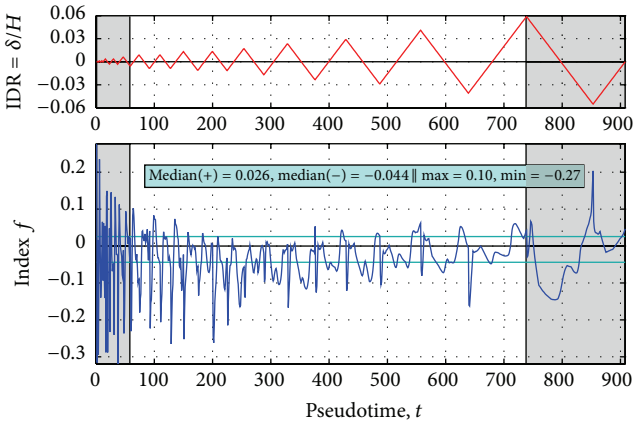


FIGURE 16: Variation of index $f$ for Pires M6 specimen.

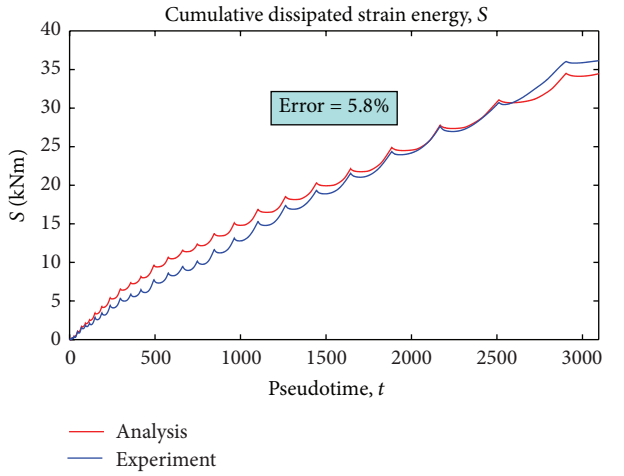


FIGURE 17: Cumulative strain energy comparison for Pires M6 specimen.

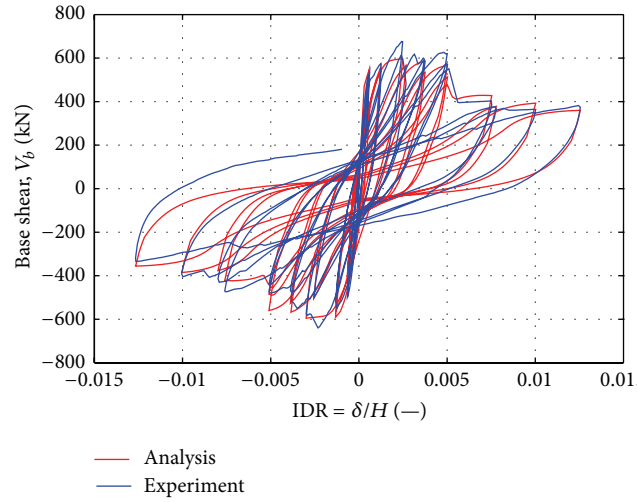


FIGURE 18: Colorado T1 specimen.

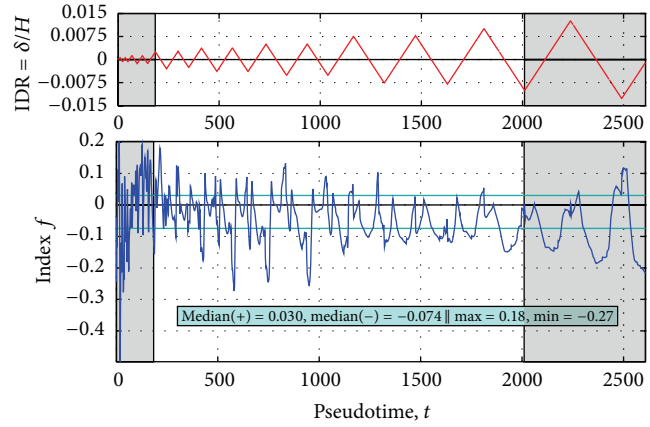


FIGURE 19: Variation of index $f$ for Colorado T1 specimen.

3% is reached and underestimated in the following cycles (Figure 17). The final average error is calculated at 5.2%, revealing that the total energy dissipated throughout the experiment is reproduced well.

The response of an even stronger masonry infill is examined by the case of Colorado T1 specimen. A satisfactory fit is achieved in the numerical model as depicted in Figures 18 and 19. The measure of the over- and underestimation indices is calculated at 3.0% and −7.4%, respectively, while the variation of index $f$ is within the (−0.27, 0.18) range.

It is important to note that a shear-dominated failure mechanism appeared in the frame members during the test at quite early stages of the loading history, limiting the ability of the proposed model to accurately capture the response of the system. More specifically, the rapid decrease of the strength of the structure noticed at +0.5% drift is a result of the formation of a wide shear crack in the top east column of the specimen, followed by another shear crack at the lower east and top west columns during the next half cycle. Such failure mechanism cannot be reproduced with the fiber elements used in the present study. Nonetheless, the general behavior of the infilled frame system is—up to that point—represented adequately.

The comparison of cumulative strain energies derived by the experimental and analytical data is illustrated in Figure 20. It is observed that a similar pattern as in the case of Pires M6 specimen discussed previously is encountered also in the case of Colorado T1 specimen. The average error is equal to 5.6%, which proves a very satisfying match between the experiment and the analysis, as far as energy dissipation is concerned.

Finally, the response of the 3-storey infilled frame tested by Koutas et al. is compared to the analytically obtained results. The final half cycle of the response is excluded from the comparison, as a shear failure mechanism that occurred to the west column is responsible for the divergence between the experimental and the numerical results from that point onwards. As presented in Figures 21 and 22, the global behavior of the numerical model shows satisfactory agreement with the experimental results. The median over- and underestimation indices are calculated as 6.2% and

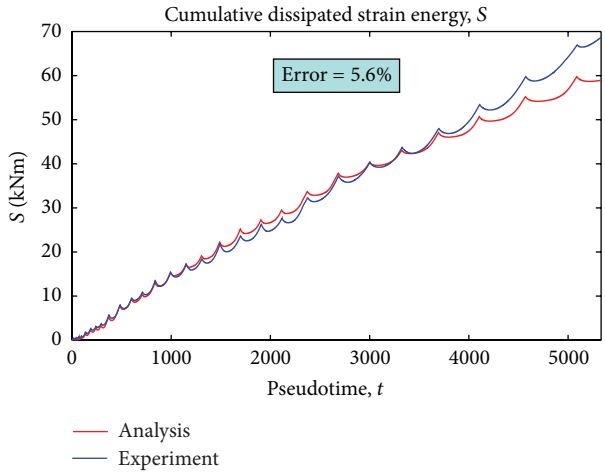


FIGURE 20: Cumulative strain energy comparison for Colorado T1 specimen.

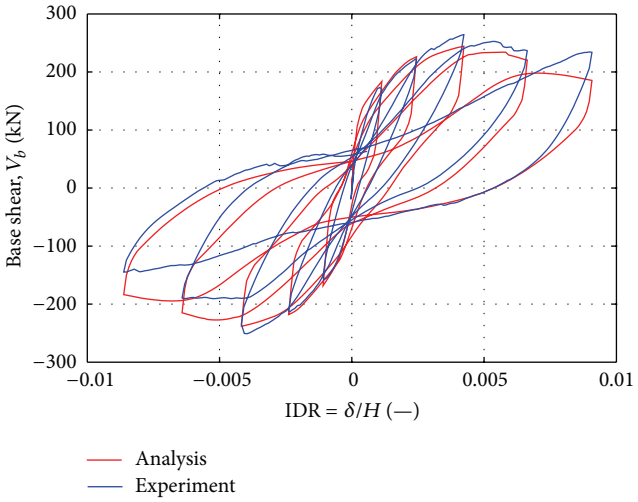


FIGURE 21: Koutas et al. U1 specimen.

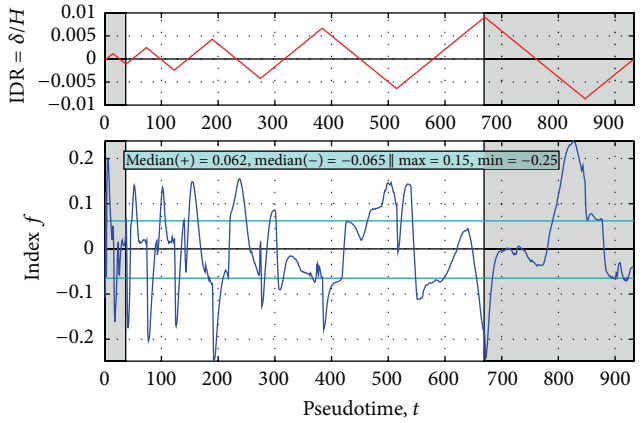


FIGURE 22: Variation of index $f$ for Koutas et al. U1 specimen.

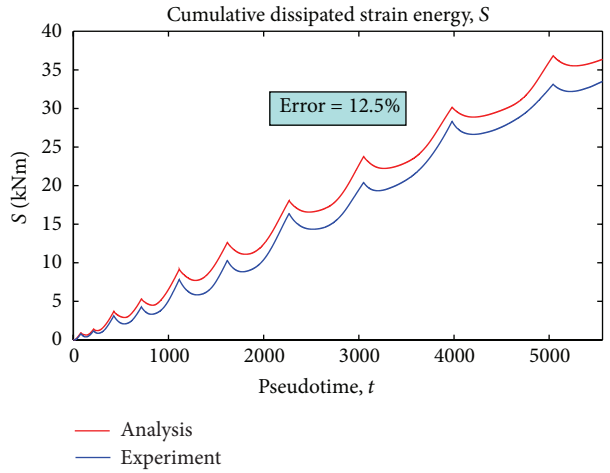


FIGURE 23: Cumulative strain energy comparison for Koutas et al. U1 specimen.

−6.5%, respectively, while the range of $f$-index lies on (−0.25, 0.15).

The strain energy dissipated in the numerical simulation seems to overestimate the actual energy dissipated during the experiment (Figure 23). The average error is 12.7% which can be considered acceptable.

An interesting outcome of the present comparison is that not only is the global behavior of the infilled frame system adequately reproduced, but also the individual response of each floor is captured quite well. The relations between the shear force at the 1st, 2nd, and 3rd floors and the corresponding (absolute) floor displacement are illustrated in Figure 24. The magnitude of the shear force in each floor and the concentration of damage in the level of the 1st floor are represented in sufficient accuracy. Some deviation from the experimental results that is more evident in the shear force-displacement response of the 1st floor is attributed to the propagation of a shear crack at the top of the 1st floor west column and therefore should not be considered as a deficiency of the proposed model.

*3.3. Parametric Investigation.* A parametric study has been conducted to investigate the sensitivity of the numerical results to the various material parameters involved in model. The study considered all the empirical parameters as well as some of the mechanical properties and was implemented using the numerical simulation of Pires M2 specimen. The parameters were individually varied, keeping all the other quantities fixed to the value used in the calibrated model presented in the previous section. Some of the modeling parameters, although examined during the parametric process, are not included in the following discussion as their influence was found to be negligible.

In order to quantify the influence of a certain parameter on the structural response, the index $f$, defined in (15), is calculated and compared for all the variations of the considered parameter. The results of this comparative procedure for the most influential of the investigated parameters (Figure 25) are presented as a comparative plot for each parameter, with the

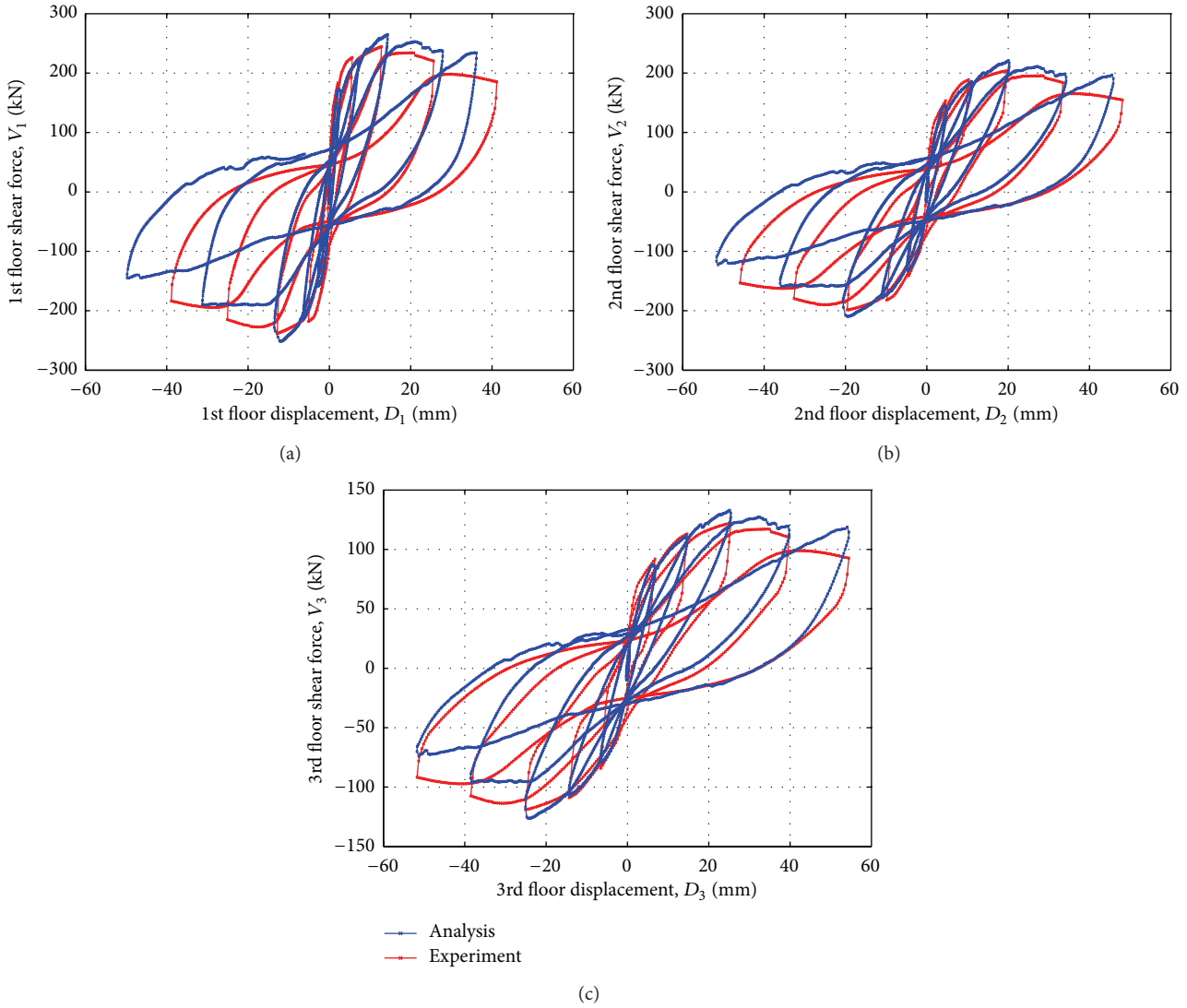


FIGURE 24: Koutas et al. U1 specimen. Floor shear force versus floor displacement (absolute) comparative results: (a) 1st floor, (b) 2nd floor, and (c) 3rd floor.

variation of the value of the parameter under investigation presented on the horizontal axis. On the vertical axis, four values of index $f$ are reported, that is, the positive and negative medians as well as the maximum and minimum $f$-values. A red dashed line is used to indicate the selected parameter-value used in the model presented in Section 3.2.

The parameters that were found to have an important impact on the response are (i) the strut area reduction factor, $A_{\text{red}} = w_2/w_1$; (ii) parameter $a_1$ controlling the end of the elastic branch on the shear spring; (iii) parameter $\gamma$ defining the proportion of the initial panel stiffness assigned to the shear spring; (iv) ultimate drift level $\text{IDR}_3$; (v) parameter $G_{\text{un}}$ which controls the unloading stiffness on the strut; (vi) parameter $A_{\text{re}}$ controlling the reloading stiffness on the strut; (vii) parameter $L_S$ that imposes strength deterioration on the shear spring response; and (iix) parameter $c_S$ that controls the rate of strength deterioration on the shear spring.

As expected, the reduction of the effective width of the diagonal strut seems to be one of the most influential parameters. Nevertheless, the selection of the area reduction factor, $A_{\text{red}}$, proposed in Section 2.3.4, is not arbitrary, but it takes into account the relative panel-to-frame stiffness. The procedure has led to the use of $A_{\text{red}} = 0.7$ in the calibrated model that is verified by the parametric study conducted here.

The estimated response is also very sensitive to the selection of parameter $a_1$. The extent of the elastic branch of the shear spring behavior is decisive for the initial stage of the response. Higher values of the parameter amplify the resistance of the infill at low-level drifts, which is confirmed by the higher values of the index $f$ that correspond to $a_1 = 0.6$ or even better to $a_1 = 0.8$.

Parameter $\gamma$ seems to have a significant impact on the response of the system as well. It can be observed that the maximum level of underestimation can vary from −26.9% for $\gamma = 0.2$ to −20.8% for $\gamma = 0.6$ and to −24.3% for $\gamma = 0.8$. The overestimation percentage is 11.4%, 9.9%, and 14.0%, respectively. However, the selection of the appropriate $\gamma$-parameter is highly dependent on the selection of the effective

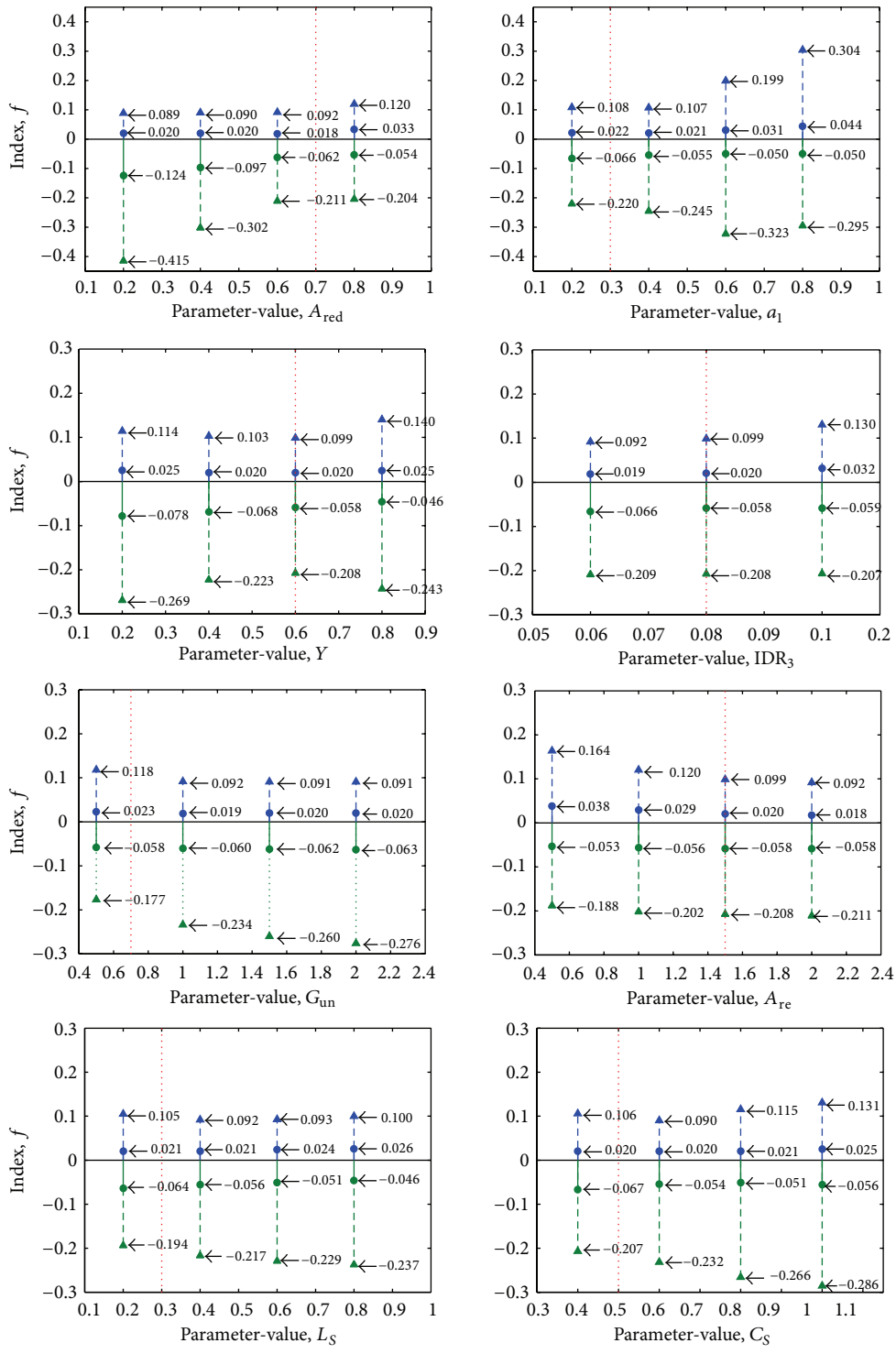


Figure 25: Parametric investigation of M2 specimen by Pires.

width of the strut, $w_1$, and the yielding force on the shear spring, $F_y$, controlled by $a_1$-parameter. Thus, the results from the variation of $\gamma$-parameter alone should be treated with caution.

The ultimate drift, IDR$_3$, is also of importance for the determination of the response. Applying higher values of ultimate drift capacity, index $f$ exhibits a shift in the positive direction, denoting overestimation conditions. Nonetheless, the relevant results illustrated in Figure 25 are quite conservative, since they do not capture the final stages of the response where the IDR$_3$-value applied is even more influential.

Among the various empirical parameters used to define the hysteretic response of the diagonal struts, the global response of the infilled frame system is more sensitive in $G_{un}$

and $A_{re}$, controlling the unloading and reloading stiffness, respectively. Actually, it seems that the use of a lower value for $G_{un}$ (≈1.0) and a higher value for $A_{re}$ (≈1.5), compared to the values suggested by Crisafulli (Table 1), yields better fit to the experimental data.

Parameters $L_S$ and $c_S$ which control the deterioration of strength of the shear spring element are also crucial. Variation of $L_S$ from 0.2 to 0.8 results in quite smooth modification of $f$-indices, while that of $c_S$ from 0.4 to 1.0 is relatively more drastic.

Finally, based on the parametric investigation of M2 specimen by Pires and the numerical results obtained from the analysis of all the considered specimens, generalized conclusions are drawn regarding the selection of the material parameters incorporated in the proposed model.

(i) A number of parameters can be characterized as noncritical and thus assigned a fixed value: $A_{ch} = 0.3$, $B_a = 1.0$, $B_{ch} = 0.9$, $G_{plu} = 1.0$, $G_{plr} = 1.1$, $e_1 = 3.0$, $e_2 = 1.0$, $\varepsilon_{cl} = 0.002$, and $f_t' = 0.05$ MPa.

(ii) The values of the parameters $f_m'$ and $A_{red} = w_2/w_1$ calculated according to the relevant formulas presented in Section 2.3 yield satisfactory results.

(iii) Appropriate values for parameter $\varepsilon_m'$, referring to the strain at maximum strength on the strut, fall within (−0.0005, −0.0001) range of values.

(iv) For parameter $\gamma$, defining the distribution of the panel stiffness among the strut and shear spring elements, values in the range of 0.6–0.7 are suggested.

(v) Parameter $a_1$ is dependent on the selection of $\gamma$-parameter, as they both control the yielding force and displacement on the shear spring. Values between 0.25 and 0.35 result in satisfactory fit to the experimental data.

(vi) Higher values than the ones suggested by Crisafulli (Table 1) are proposed for parameter $A_{re}$. Values within (0.8, 1.5) are considered more suitable.

(vii) The suggested values for parameter $G_{un}$ fall within (0.5, 0.7) range, lower than the corresponding range proposed by Crisafulli (Table 1).

(viii) Parameter $L_S$, controlling strength deterioration, should be taken between 0.3 and 0.4, while the rate of strength deterioration, controlled by $c_S$-parameter, varies between 0.5 and1.0.

(ix) Parameter $L_K$, controlling unloading stiffness deterioration, can be deactivated (assignment of a high value, e.g., $L_K = 1000$) to reduce the unknown quantities incorporated in the model. However, given the characteristics of the masonry infill studied, $L_K$ values between 0.2 and 0.3 should be used when unloading stiffness deterioration is expected to be more pronounced. Specimens T1 at Colorado, U1 by Koutas et al., and M6 by Pires, in which a stronger infill was employed, constitute such cases. Unity can be adopted for the rate of unloading stiffness deterioration, $c_K$.

(x) The variance of $IDR_1$ (0.021%–1.0%) and $IDR_2$ (0.55%–2.5%) levels used in the present study is indicative of their high dependence on the characteristics of the masonry infill and the surrounding frame and impedes the suggestion of a feasible range of values for practical applications.

(xi) $IDR_3$-parameter, controlling the ultimate state of the infill response, can be assigned a value between 5% and 8%.

## 4. Conclusions

The paper presents an approach for assessing the nonlinear response of masonry infilled RC frames under in-plane lateral loads. The model, based on the masonry panel by Crisafulli, combines three elements to provide a relatively accurate representation of the global behavior of the infill panel. The constitutive models adopted for each element involve a number of parameters, either empirical or linked to the mechanical properties of the infill. A procedure for the evaluation of the various parameters is established, followed by the validation of the proposed methods with available experimental data.

The comparison between experimental data and numerical results is conducted on the basis of two quantities: (i) the dimensionless index $f$ that is basically the difference in the base shear (at the same displacement levels) divided by the maximum experimentally obtained base shear and (ii) the average error in the cumulative strain energy dissipated by the numerical model and the actual specimen.

It is concluded that the model can adequately reproduce the load-displacement response exhibited by infilled RC frames. The medians of the positive and negative $f$-values, indicating overestimation and underestimation conditions, respectively, vary from 2.0% to 7.4%, proving a satisfying fit to the experimental data. The error in the dissipated strain energy is also acceptable, ranging from 5.2% to 14.9%.

In addition, a parametric study, carried out to evaluate the sensitivity of the numerical results to the selection of the modeling parameters (especially those with empirical nature), shows that only few of the parameters show a significant impact on the overall response, providing evidence that a possible reduction of the unknown and noneasily identified parameters could be considered.

Based on the results of both the parametric investigation and the analysis of the individual specimens considered, proposals regarding appropriate selection of the parameters employed in the model are provided.

## Conflict of Interests

The authors declare that there is no conflict of interests regarding the publication of this paper.

## References

[1] F. J. Crisafulli and A. J. Carr, "Proposed macro-model for the analysis of infilled frame structures," *Bulletin of the New Zealand*

*Society for Earthquake Engineering*, vol. 40, no. 2, pp. 69–77, 2007.

[2] H. R. Lotfi, *Finite element analysis of fracure of concrete and masonry structures, [Ph.D. dissertation]*, University of Colorado, Boulder, Colorado, 1992.

[3] P. B. Lourenco, *Computational strategies for masonry structures, [Ph.D. dissertation]*, Delft University of Technology, Delft, The Netherlands, 1996.

[4] M. M. Attard, A. Nappi, and F. Tin-Loi, "Modeling fracture in masonry," *Journal of Structural Engineering*, vol. 133, no. 10, pp. 1385–1392, 2007.

[5] A. B. Mehrabi and P. B. Shing, "Finite element modeling of masonry-infilled RC frames," *Journal of Structural Engineering*, vol. 123, no. 5, pp. 604–613, 1997.

[6] Y.-J. Chiou, J.-C. Tzeng, and Y.-W. Liou, "Experimental and analytical study of masonry infilled frames," *Journal of Structural Engineering*, vol. 125, no. 10, pp. 1109–1117, 1999.

[7] A. Stavridis and P. B. Shing, "Finite-element modeling of nonlinear behavior of masonry-infilled RC frames," *Journal of Structural Engineering*, vol. 136, no. 3, pp. 285–296, 2010.

[8] S. V. Polyakov, "On the interaction between masonry filler walls and enclosing frame when loaded in the plane of the wall," in *Translation in Earthquake Engineering*, pp. 36–42, Earthquake Engineering Research Institute (EERI), San Francisco, Calif, USA, 1960.

[9] M. Holmes, "Steel frames with brickwork and concrete infilling," *ICE Proceedings*, vol. 19, no. 4, pp. 473–478, 1961.

[10] B. S. Smith, "Lateral stiffness of infilled frames," *Journal of Structural Engineering*, vol. 88, no. 6, pp. 182–199, 1962.

[11] R. J. Mainstone, "On the stiffnesses and strengths of infilled frames," *ICE Proceedings*, vol. 49, no. 2, p. 230, 1971.

[12] C. A. Syrmakezis and V. Y. Vratsanou, "Influence of infill walls to RC frames response," in *Proceedings of the 8th European Conference on Earthquake Engineering of the European Association for Earthquake Engineering (EAEE)*, pp. 47–53, Instabul, Turkey, 1986.

[13] C. Z. Chrysostomou, P. Gergely, and J. F. Abel, "A six-strut model for nonlinear dynamic analysis of steel infilled frames," *International Journal of Structural Stability and Dynamics*, vol. 2, no. 3, pp. 335–353, 2002.

[14] W. W. El-Dakhakhni, M. Elgaaly, and A. A. Hamid, "Three-strut model for concrete masonry-infilled steel frames," *Journal of Structural Engineering*, vol. 129, no. 2, pp. 177–185, 2003.

[15] M. N. Fardis and T. B. Panagiotakos, "Seismic design and response of bare and masonry-infilled reinforced concrete buildings. Part II: infilled structures," *Journal of Earthquake Engineering*, vol. 1, no. 3, pp. 475–503, 1997.

[16] F. J. Crisafulli, *Seismic behavior of reinforced concrete structures with masonry infills, [Ph.D. dissertation]*, Department of Civil Engineering, University of Cantebury, Cantebury, New Zealand, 1997.

[17] S. Mazzoni, F. McKenna, M. H. Scott, and G. L. Fenves, *Open System for Earthquake Engineering Simulation (OpenSees), User Command-Language Manual*, Pacific Earthquake Engineering Research Center, University of California, Berkeley, Calif, USA, 2006, http://opensees.berkeley.edu/OpenSees/manuals/.

[18] J. B. Mander, M. J. N. Priestley, and R. Park, "Theoretical stress-strain model for confined concrete," *Journal of Structural Engineering*, vol. 114, no. 8, pp. 1804–1826, 1988.

[19] E. Smyrou, C. Blandon, S. Antoniou, R. Pinho, and F. Crisafulli, "Implementation and verification of a masonry panel model for nonlinear dynamic analysis of infilled RC frames," *Bulletin of Earthquake Engineering*, vol. 9, no. 5, pp. 1519–1534, 2011.

[20] D. G. Lignos and H. Krawinkler, "Deterioration modeling of steel components in support of collapse prediction of steel moment frames under earthquake loading," *Journal of Structural Engineering*, vol. 137, no. 11, pp. 1291–1302, 2011.

[21] D. G. Lignos and H. Krawinkler, "Sidesway collapse of deteriorating structural systems under seismic excitations," Tech. Rep. TB177, The John A. Blume Earthquake Engineering Research Center, Stanford University, Stanford, Calif, USA, 2012.

[22] M. N. Fardis, "Experimental and numerical investigations on the seismic response of RC frames and recommendations for Code Provisions," Tech. Rep. 6, ECOEST PREEC8, 1997.

[23] S. H. Bertoldi, L. D. Decanini, and C. Gavarini, "Telai tamponati soggetti ad azione sismica, un modelo semplificato: confronto sperimentale e numerico," in *Atti del 6 Convegno Nazionale ANIDIS*, Perugia, Italy, 1993, (Italian).

[24] T. Pauley and M. J. N. Priestley, *Seismic Design of Reinforced Concrete and Masonry Buildings*, Wiley, New York, NY, USA, 1992.

[25] L. D. Decanini and G. E. Fantin, "Modelos simplificados de la mamponesteria incluida en porticos. Caracteristicas de rigidez y resistencia lateral en astado limite," in *Jornadas Argentinas de Ingenieria Estructural III*, vol. 2, pp. 817–8605, Asociacion de Ingenieros Estructurales, Buenos Aires, Argentina, (Spanish).

[26] F. M. G. Pires and E. C. Carvalho, "The behaviour of infilled reinforced concrete frames under horizontal cyclic loading," in *Proceedings of the 10th World Conference on Earthquake Engineering*, vol. 6, pp. 3419–33422, Balkema, Rotterdam, 1992.

[27] F. M. G. Pires, *Influencia das paredes de alvenaria no comportamento de estruturas reticuladas de betao armado sujeitas a accoes horizontais [Ph.D. dissertation]*, National Laboratory in Civil Engineering, Lisbon, Portugal, 1990, (Portugese).

[28] M. Kyriakides, *Numerical analysis of unreinforced masonry infills in non-ductile reinforced concrete frames using Engineered Cementitious Composites, [Ph.D. dissertation]*, Stanford University, Stanford, Calif, USA, 2011.

[29] I. Koutromanos, *Numerical analysis of masonry—infilled RC frames subjected to seismic loads and experimental evaluation of retrofit techniques, [Ph.D. dissertation]*, University of California, San Diego, Calif, USA, 2011.

[30] L. Koutas, S. N. Bousias, and T. C. Triantafillou, "In-plane behavior of a three-strorey masonry infilled RC frame," in *Proceedings of the 4th International fib Congress*, Mumbai, India, February 2014.